Estimation of surface energy fluxes in the Arctic tundra using the remote sensing thermal-based Two-Source Energy Balance model

Jordi Cristóbal[1,2], Anupma Prakash[1], Martha C. Anderson[3], William P. Kustas[3], Eugénie S. Euskirchen[4], Douglas L. Kane[2]

[1]Geophysical Institute. University of Alaska Fairbanks, Fairbanks, Alaska, 99775,USA
[2]Institute of Northern Engineering. Water Environmental Research Center, University of Alaska Fairbanks, Fairbanks, Alaska, 99775, USA
[3]Hydrology and Remote Sensing Laboratory, United States Department of Agriculture, Agriculture Research Service, Beltsville, Maryland, 20705, USA
[4]Institute of Arctic Biology. University of Alaska Fairbanks, Fairbanks, Alaska, 99775, USA

Correspondence to: Jordi Cristóbal (j.cristobal@alaska.edu)

Abstract. The Arctic has become generally a warmer place over the past decades leading to earlier snow melt, permafrost degradation and changing plant communities. Increases in precipitation and local evaporation in the Arctic, known as one of the acceleration components of the hydrologic cycle, coupled with land cover changes, have resulted in significant changes in the regional surface energy budget. Quantifying spatiotemporal trends in surface energy flux partitioning is a key to forecasting ecological responses to changing climate conditions in the Arctic regions. An extensive evaluation of the two-source energy balance model (TSEB) - a remote sensing-based model using thermal infrared retrievals of land-surface temperature - was performed using tower measurements collected over different tundra types in Alaska in all sky conditions over the full growing season from 2008 to 2012. Based on comparisons with flux tower observations, refinements in the original TSEB net radiation, soil heat flux and canopy transpiration parameterizations were identified for the unique Arctic tundra conditions. In particular, a revised method for estimating soil heat flux based on relationships with soil temperature was developed, resulting in significantly improved performance. These refinements result in mean flux errors around 50 W·m^{-2} at half-hourly timesteps similar to errors typically reported in surface energy balance modelling studies conducted in more temperate climatic regimes. MODIS LAI remote sensing product proved to be useful for estimating energy fluxes in Arctic tundra in the absence of field data. This work builds toward a regional implementation of the TSEB model over Arctic tundra ecosystems, using thermal satellite remote sensing to assess response of surface fluxes to changing vegetation and climate conditions.

1 Introduction

Near-surface or shelter level air temperatures in the Alaskan Arctic have shown a significant increase, especially in past decade (Serreze and Barry, 2011). Results from models forced with a range of climate scenarios from the Intergovernmental Panel on Climate Change (IPCC) indicate that by the mid-21st century the permafrost area in the Northern Hemisphere is

likely to decrease by 20–35% (Bates et al., 2008). In general, the Arctic has become a warmer place, leading to an acceleration of the hydrologic cycle, earlier snow melt, drier soils due to permafrost degradation (ACIA, 2004; AMAP, 2012; Lammers et al., 2001; Vörösmarty et al., 2001; Elmendorf et al., 2012; Rawlins et al., 2010; Sturm et al., 2001; Overduin and Kane, 2006; Arendt et al., 2002). Furthermore, the hydrologic response of the Arctic land surface to changing

5   climate is dynamically coupled to the region's surface energy balance (Vörösmarty et al., 2001), and its partitioning plays an important role in modulating the hydrologic cycle of Arctic basins (Rawlins et al., 2010).

Evapotranspiration (ET, in units of mass, kg s^{-1} m^{-2} or mm d^{-1}) or equivalently, latent heat flux (LE, in energy units, W·m^{-2}), is an important component of both the land surface hydrologic cycle and surface energy balance. As an example, Kane et al. (2004) reported water loss due to ET in the Imnavait Creek Basin in Alaska is about 74% of summer precipitation or 50% of

10   annual precipitation, as estimated from water balance computations. Even though ET is a significant component of the hydrologic cycle in Arctic regions, it is poorly quantified in Arctic basins, and the bulk estimates do not accurately account for spatial and temporal variability due to vegetation type and topography (Kane and Yang, 2004). In the Arctic, values of ET or LE are usually either derived from field estimates (Kane et al., 1990;Mendez et al., 1998) or calculated purely from empirical or quasi-physical models such as those described by Zhang et al. (2000) and Shutov et al. (2006) using

15   meteorological station forcing data. However, due to remoteness, harsh winter conditions and the high costs of maintaining ground-based measurement networks, the data currently collected are also inconsistent both temporally and spatially.

Over at least the past three decades, Arctic ecosystems have shown evidence of "greening" (Xu et al., 2013;Jia et al., 2003), with about a 14% increase in peak vegetation for the Arctic tundra biome (Bhatt et al., 2010). In Arctic tundra ecosystems, several factors have contributed to the vegetation change such as increased extent of severe fires, increased extent in

20   deciduous vegetation or shrub encroachment in tundra ecosystems (Myers-Smith et al., 2011;Sturm et al., 2001), among others. Moreover, the forest-tundra transition zone is continually observed further north, tree heights are increasing, and shrubs are becoming denser and taller (ACIA, 2004;AMAP, 2012). These changes in vegetation will have an important impact on the surface energy balance, especially in areas where shrubs have made their appearance in former tundra vegetation. This increase in leaf area index, together with canopy height, and changes in the distribution of canopy elements,

25   will augment the multiple scattering and absorption of radiation, likely resulting in a lower albedo (Beringer et al., 2005). Also according to Beringer et al. (2005), Bowen ratio increases from tundra to forested sites will result in an increasing dominance of sensible heat (H) as the primary energy source heating the atmosphere. In the case of a transition from tundra to tall shrub and then to forest, H would likely increase during the growing season from ~15% to nearly 30%, respectively. This will have an important impact in the tundra energy partitioning, resulting in a positive feedback to the atmosphere that

30   further warms the Arctic climate. However, the magnitude of changes in surface energy partitioning due to vegetation changes and resulting impact on local Arctic climate is still unclear and more research is needed to better understand these vegetation change-atmosphere dynamics (Eugster et al., 2000;Jung et al., 2010).

In the last two decades, surface energy balance methods have demonstrated their utility in modelling water availability using diagnostic retrievals of energy fluxes from *in situ* or remote sensing data, especially data acquired in the thermal infrared region (Kalma et al., 2008). While remote sensing estimates of ET over the Arctic exist from global modelling systems (Mu et al., 2009;Zhang et al., 2010), these systems typically do not compute the full energy balance. To estimate energy fluxes at

5 local scales, on the order of hundreds of meters, initiatives such as FLUXNET (http://fluxnet.ornl.gov/) provide eddy covariance flux measurements at discrete sites situated in different ecosystems across the U.S. and globally. Unfortunately, there are few measurements sites in the Arctic (Mu et al., 2009), making the existing instrument network insufficient to capture pertinent details of the changing Arctic climate and landscape (ACIA, 2004; AMAP, 2012; Serreze and Barry, 2011; Vörösmarty et al., 2001). Consequently, there is a strong need to focus on refining and evaluating models providing spatial-

10 distributed fluxes to facilitate more accurate spatio-temporal mapping of Arctic energy fluxes.

The aim of this work is to evaluate the performance of a remote sensing energy balance approach, forced primarily by measurements of land-surface temperature, in estimating surface energy fluxes during Arctic tundra growing season. The Two-Source Energy Balance (TSEB) model, proposed by Norman et al. (1995), has been demonstrated to work well over a range in vegetation and climate conditions, but has not yet been examined for tundra ecosystems at high latitudes. This

15 TSEB land surface scheme has been coupled to a regional modelling system using geostationary and polar orbiting satellite data providing regional and continental scale fluxes and thus could potentially be applied to the Arctic for monitoring and mapping the surface energy balance (Anderson et al., 2011). In this study, the TSEB is run locally using in situ forcing data from three eddy covariance flux towers in all sky conditions (including clear sky, partially cloudy and overcast conditions) over Alaskan tundra sites during the growing season from 2008 to 2012. Vegetation amount is quantified using leaf area

20 index data from the Moderate Resolution Imaging Spectroradiometer (MODIS). The modelled energy balance is compared with measurements at three flux sites to ascertain modifications required to enhance performance over tundra ecosystems.

2 Two-Source Energy Balance model: an overview

Evapotranspiration (ET) can be estimated by surface energy balance models that partition the energy available at the land surface (R_N - G, where R_N is net radiation and G is the soil heat flux, both in $W \cdot m^{-2}$) into turbulent fluxes of sensible and

25 latent heating (H and LE, respectively, in $W \cdot m^{-2}$):

$$LE + H = R_N - G, \tag{1}$$

where L is the latent heat of vaporization ($J\ kg^{-1}$) and E is ET ($kg\ s^{-1}\ m^{-2}$ or $mm\ s^{-1}$).

The model used in this study is the series version of the Two-Source Energy Balance (TSEB) scheme originally proposed by Norman et al. (1995), which has been revised to improve shortwave and longwave radiation exchange within the soil–

30 canopy system and the soil–canopy energy exchange (Kustas and Norman, 1999, 2000). A list of the TSEB inputs can be found in Table 1. TSEB has been successfully applied over rainfed and irrigated crops and grasslands in temperate and semi-

arid climates (Anderson et al., 2012;Anderson et al., 2004;Cammalleri et al., 2012, 2010) but has not been previously applied over the Arctic tundra.

In the TSEB, directional surface radiometric temperature derived from satellite or a ground-based radiometer, $T_{RAD}(\theta)$ (K), is considered to be a composite of the soil and canopy temperatures, expressed as:

$$T_{RAD}(\theta) \approx [f_c(\theta)T_c^4 + (1 - f_c(\theta))T_s^4]^{1/4}, \tag{2}$$

where T_C is canopy temperature (K), T_S is soil temperature (K), and $f_C(\theta)$ is the fractional vegetation cover observed at the radiometer view angle θ. For a canopy with a spherical leaf angle distribution and leaf area index LAI, $f_C(\theta)$ can be estimated as:

$$f_c(\theta) = 1 - exp\left(\frac{-0.5\Omega LAI}{cos\theta}\right), \tag{3}$$

where the factor Ω indicates the degree to which vegetation is clumped as in rowcrops or sparsely vegetated shrubland canopies (Kustas and Norman, 1999, 2000). The composite soil and canopy temperatures are used to compute the surface energy balance for the canopy and soil components of the combined land-surface system:

$$R_{NS} = H_S + LE_S + G, \tag{4}$$

$$R_{NC} = H_C + LE_C, \tag{5}$$

where R_{NS} is net radiation at the soil surface, R_{NC} is net radiation divergence in the vegetated canopy layer, H_C and H_S are canopy and soil sensible heat flux, respectively, LE_C is the canopy transpiration rate, LE_S is soil evaporation, and G is the soil heat flux. The net shortwave radiation is calculated from the measured incoming solar radiation and the surface albedo, while net longwave radiation is estimated from the observed air and land surface temperatures, using the Stefan-Boltzmann equation with atmospheric emissivity from the Brutsaert (1975) method.

By permitting the soil and vegetated canopy fluxes to interact with each other, Norman et al. (1995) derived expressions for H_S and H_C expressed as a function of temperature differences where:

$$H_S = \rho C_p \frac{T_S - T_{AC}}{R_S}, \tag{6}$$

and

$$H_C = \rho C_p \frac{T_C - T_{AC}}{R_X}, \tag{7}$$

with the total sensible heat flux $H = H_C + H_S$ expressed as

$$H = \rho C_p \frac{T_{AC} - T_A}{R_A}, \tag{8}$$

where ρ is air density (kg·m^{-3}), C_p is the specific heat of air (kJ·kg^{-1}·K^{-1}), T_{AC} is air temperature in the canopy air layer (K), T_A is the air temperature in the surface layer measured at some height above the canopy (K), R_X is the total boundary layer resistance of the complete canopy of leaves (s m^{-1}), R_S is the resistance to sensible heat exchange from the soil surface (s m^{-1}) and R_A is aerodynamic resistance (s m^{-1}) defined by:

$$R_A = \frac{[ln((z_U - d_O)/z_{OM}) - \Psi_M][ln((z_T - d_O)/z_{OM}) - \Psi_H]}{k^2 u}, \tag{9}$$

In Eq. (9) d_O is the displacement height, u is the wind speed measured at height z_U, k is von Karman's constant (≈0.4), z_T is the height of the T_A measurement, Ψ_M and Ψ_H are the Monin–Obukhov stability functions for momentum and heat, respectively, and z_{OM} is the aerodynamic roughness length.

The original resistance formulations are described in more detail in Norman et al. (1995) with revisions described in Kustas and Norman (1999) and Kustas and Norman (2000). Weighting of the heat flux contributions from the canopy and soil components is performed indirectly by the partitioning of the R_N between soil and canopy and via the impact on resistance values from the fractional amount and type of canopy cover (see Kustas and Norman, 1999).

For the latent heat flux from the canopy, the Priestley–Taylor formula is used to initially estimate a potential rate for LE_C:

$$LE_C = \alpha_{PTC} f_G \frac{\Delta}{\Delta + \gamma} R_{NC}, \tag{10}$$

where α_{PTC} is a variable quantity related to the Priestley–Taylor coefficient (Priestley and Taylor, 1972), but in this case defined exclusively for the canopy component, which was suggested for row crops by Tanner and Jury (1976) and normally set to an initial value of 1.2, f_G is the fraction of green vegetation, Δ is the slope of the saturation vapour pressure versus temperature curve and γ is the psychrometric constant (~0.066 kPa °C^{-1}). Under stress conditions, TSEB iteratively reduces α_{PTC} from its initial value (a thorough discussion of conditions that force a reduction in α_{PTC}, can be found in Anderson et al. (2005) and Li et al. (2005)).

The latent heat flux from the soil surface is solved as a residual in the energy balance equation:

$$LE_S = R_{NS} - G - H_S, \tag{11}$$

with G estimated as a fraction of the net radiation at the soil surface (c_G):

$$G = c_G R_{NS}, \tag{12}$$

From midmorning to midday period, when daytime TIR satellite imagery is typically acquired, the value of c_G can be typically assumed to be constant (Kustas and Daughtry, 1990;Santanello and Friedl, 2003). In this case, a typical value of ~0.3 can be assumed for c_G based on experimental data from several sources (Daughtry et al., 1990). However, c_G value

varies with soil type and moisture conditions as well as time, due to the phase shift between G and R_{NS} over a diurnal cycle (Santanello and Friedl, 2003).

3 TSEB formulation refinements for Arctic tundra

3.1 Downwelling longwave radiation estimation: effective atmospheric emissivity for all sky conditions

The original TSEB formulation estimates the downwelling longwave radiation component of R_N using the effective atmospheric emissivity (ε) method described in Brutsaert (1975) for clear sky conditions:

$$\varepsilon = C(e/T_A)^{1/7},\tag{13}$$

where e is the water pressure in millibars and T_A in K and C is 1.24 as in the original Brutsaert (1975) formulation. However, in this study TSEB is applied for all sky conditions, including clear sky, partially cloudy and overcast conditions. To estimate ε for all sky conditions Crawford and Duchon (1999) proposed a methodology that incorporated the Brutsaert (1975) clear-sky parameterization and the Deardorff (1978) cloudiness correction using a simple cloud modification introducing a cloud fraction term (clf) according to the following equation:

$$\varepsilon = \left\{ clf + (1 - clf)\left[C(e/T_A)^{1/7} \right] \right\},\tag{14}$$

The clf is defined as:

$$clf = 1 - s,\tag{15}$$

where s is the ratio of the measured solar irradiance to the clear-sky irradiance. Shortwave clear-sky irradiance used in Eq. (15) may be obtained through the methodology proposed by Pons and Ninyerola (2008), where incident clear-sky irradiance is calculated through a digital elevation model at a specific point during a particular day of the year taking into account the position of the Sun, the angles of incidence, the projected shadows, the atmospheric extinction and the distance from the Earth to the Sun.

For Arctic areas Jin et al. (2006) suggested an improved formulation of C for clear sky conditions that can also be applied in Eq. (14) for all sky conditions, defined as:

$$C = 0.0003(T_A - 273.16)^2 - 0.0079(T_A - 273.16) + 1.2983,\tag{16}$$

In order to evaluate if the Jin et al. (2006) method offered more accurate estimates of ε for Arctic conditions, this method was compared to Brutsaert (1975) formulation used in TSEB, in both cases for all sky conditions using Eq. (14).

3.2 Soil heat flux parameterization: c_G coefficient

Currently there are several methodologies that allow estimating soil heat flux from tenths of centimetres to meters in depth in the Arctic tundra by using modelling or instrumentation at several depths (Lynch et al., 1999;Ekici et al., 2015;Jiang et al., 2015;Romanovsky et al., 1997;Yao et al., 2011;Zhuang et al., 2001;Hinzman et al., 1998). However, in this study a simple approach based on the relationship between G and R_N (Eq. (12)) was used to estimate the soil heat flux in the near-surface soil layer (around 10 cm depth). This approach has less complexity and requires less input data than the methods mentioned above and allows estimating G at regional scales.

In the Arctic tundra the propagation of the thawing front in the soil active layer consumes a large proportion (around 18%) of the energy input from the positive net radiation (Boike et al., 2008a; Rouse, 1985). Moreover, the presence of permafrost in tundra areas may contribute to the large tundra soil heat flux by creating a strong thermal gradient between the ground surface and depth, offsetting the influence of the highly insulative moss cover which would otherwise have been expected to reduce soil heat flux (Beringer et al., 2005; Blok et al., 2011). Therefore, previous formulations of soil heat flux used in TSEB applications, mainly representative of cropped and sparse-vegetated areas, need to be adjusted and validated for Arctic tundra.

In past TSEB applications, and according to Kustas and Daughtry (1990) and Santanello and Friedl (2003), while a constant value of c_G value around 0.3 can be reasonably used to estimate G for the midmorning to midday period (Eq. (12)), this assumption can result in significant errors if applied out of this time range. For diurnal hourly timescales, Kustas et al. (1998), developed a method to estimate c_G based on time differences with the local solar noon quantified by a non-dimensional time parameter, although this approach does not consider the phase shift between G and R_{NS} over a diurnal cycle. However, a phase shift was included in the model proposed by Santanello and Friedl (2003) following:

$$c_G = A\,cos[2\pi(t + S)/B]\,,\tag{17}$$

where A represents the maximum value of c_G, B is chosen to minimize the deviation of c_G from Eq. (12), t is time in seconds relative to solar noon and S is the phase shift between G and R_{NS} in seconds. Values fitted for A, S and B resulted in values of 0.31, 10 800 and 74 000, respectively.

Although c_G values for Arctic tundra were not found in the literature, several studies present the relationship between R_N and G during the summer months in similar tundra areas. Based on these studies, a mean value of 0.14, as a maximum value of c_G in Eq. (17), can be derived from different analyses of R_N and G over the Arctic tundra (Beringer et al., 2005;Eugster et al., 2005;Boike et al., 2008b; Eaton et al., 2001;Eugster et al., 2000;Kodama et al., 2007;Langer et al., 2011;Soegaard et al., 2001;Westermann et al., 2009;Mendez et al., 1998;Lund et al., 2014).

An alternative parameterization for G suggested by Santanello and Friedl (2003) for several types of soils with crops, and by Jacobsen and Hansen (1999) for Arctic tundra, links the soil heat flux to the diurnal variations in surface radiometric temperature. This approach can also be applied for Arctic tundra as follows:

$$G = c_{TG} T_{RAD},$$ (18)

5 where c_{TG} is a coefficient that represents the relationship between the diurnal variation of T_{RAD} and G. For diurnal hourly timescales, c_{TG} can be also estimated using the phase shift proposed in Eq. (17) where, in this case, S is the phase shift between G and T_{RAD} in seconds. This new approach avoids using R_{NS}, which is more difficult to define in tundra systems given the influence of the surface organic layer above the mineral soil. Moreover, A, S and B in Eq. (17) can be fitted by using direct measurements of T_{RAD} from thermal field sensors, commonly available on flux towers (pyrgeometer), or thermal

10 data from geostationary or polar satellites.

Thus, to evaluate soil heat flux for diurnal hourly timescales, Kustas et al. (1998) and Santanello and Friedl (2003) approaches were compared using the original c_G value of 0.30 and a new value for Arctic tundra of 0.14 as maximum values of c_G in Eq. (17). The new c_{TG} approach was also fitted and then compared to these radiation-based methods.1.2.1

3.3 Priestley-Taylor coefficient

15 In the original TSEB formulation, the Priestley-Taylor approach for the canopy component of LE is used. In this case α_{PTC} is normally set to an initial value of 1.26 for the general conditions tested during the growing season in rangelands and croplands. For stressed canopies, TSEB internally modifies α_{PTC} to yield reasonable partitioning between LE_C and LE_S.

As with the c_G coefficient, specific α_{PTC} values for tundra were not found in the literature. Alternatively, measurements of bulk (soil+canopy) for Arctic tundra systems are available (Beringer et al., 2005;Eaton et al., 2001;Eugster et al.,

20 2005;Engstrom et al., 2002;Mendez et al., 1998;Lund et al., 2014) suggesting a mean value of around 0.92. This bulk value might suggest that α_{PTC} could also be lower for summer Alaska tundra conditions. For natural vegetation, Agam et al. (2010) also suggested that a lower α_{PTC} value might yield better results. Therefore, for modelling purposes two different values of α_{PTC} values, 0.92 and 1.26, were applied to evaluate which nominal α_{PTC} input to TSEB was more appropriate for Arctic tundra.

25 ## 4 Study area and data description

4.1 Study area

To refine and evaluate the TSEB model for Alaska's Arctic tundra summer conditions, three eddy covariance flux towers (referred to as Fen, Tussock and Heath; see Fig. 1) were selected. These are located across the Imnavait Watershed (~904 m

a.s.l.) with eddy covariance and associated meteorological data collection beginning in 2007 (Euskirchen et al., 2012; Kade et al., 2012). A brief description of instrumentation at the tower sites is provided in Table 2.

The Fen tower, located at the valley bottom in a wet sedge ecosystem, includes *Eriophorum angustifolium* and dwarf shrubs such as *Betula nana* and *Salix* spp and vegetation types around the tower are comprised of 52% wet sedge, and 47% tussock

5   tundra. The Tussock tower, located at the midslope in a moist acidic tussock tundra ecosystem, is dominated by the tussock-forming sedge *Eriophorum vaginatum*, *Sphagnum* spp., and dwarf shrubs such as *Betula nana* and *Salix* spp. In this case, vegetation types around the flux tower are 95% tussock tundra. The Heath tower sits atop a broad dry ridge at the top edge of the watershed boundary in a heath tundra ecosystem dominated by *Dryas* spp, lichen, and dwarf shrubs. The vegetation here is 20% heath, but also included 72% tussock tundra, with the balance made of up of sedge meadow and bare soil. Further

10   detailed information about the study is provided in Euskirchen et al. (2012).

4.2 Model inputs and evaluation dataset: Micrometeorological data and vegetation-based measurements

Data incorporated in this study spanned from May to September 2008 to 2012. These included eddy covariance data for latent and sensible collected at 10 Hz and processed to 30-minute means (described below) as well as meteorological data collected at 30-minute intervals (Table 1 and Table 2). These data, from under all sky conditions, were used to refine and

15   evaluate the model performance (Table 1). This dataset was considered to be representative of the short Arctic tundra vegetative cycle from early growing to senescence as well as to capture inter- and intra-annual vegetation dynamics.

Meteorological input for TSEB include wind speed, air temperature, vapour pressure, atmospheric pressure, longwave incoming radiation and solar radiation, all of which were collected at the three measurement sites (see Table 1 and 2). The surface radiometric temperature T_{RAD} inputs were obtained from the pyrgeometer sensor at the Tussock station and from

20   infrared radiometer sensors at both Fen and Heath stations. In addition, TSEB also requires estimates of LAI and the fraction of vegetation that is green to specify f_C in Eq. (2). While, *in situ* measurements of LAI were not available at the tower sites, the MODIS LAI product (MOD15) was available for the study area. This product has been successfully applied in other applications of the TSEB (Guzinski et al., 2013) where sites are considered homogeneous over several kilometres, and serve here as a proxy for local observations, selecting the best estimates through the LAI product quality flags. The fraction of

25   vegetation that is green (f_G) in Eq. (10) was set equal to the ratio of the fraction of absorbed photosynthetically active radiation (PAR) by the green vegetation and the fraction of PAR intercepted by the total vegetation cover (Guzinski et al., 2013) using the incoming and outgoing PAR from the flux stations. Vegetation height, used to define roughness parameters d_O and z_{OM}, was assigned based on measurements made in the vicinity of the flux towers (Kade et al., 2012) and the clumping factor was set to 1 for all sites based on the knowledge that Arctic tundra has a variable organic layer with little

30   bare ground. Variability regarding these inputs for the studied periods is shown in Table 1. Moreover, to ensure that only snow-free periods were analysed, Terra/Aqua MODIS snow cover products (MOD10A1 and MYD10A1) were used to

screen days with snow cover at the beginning and end of the growing season. Future work will extend these analyses to periods with snow cover using a snow-adapted form of the TSEB (Kongoli et al., 2014).

The eddy covariance data used in TSEB evaluation, including latent and sensible heat, were processed to account for changes in mass flow caused by changes in air density (Webb et al., 1980). Corrections for frequency attenuation of eddy covariance fluxes following Massman (2000) and Rannik (2001) and storage corrections for calm periods suggested by Rocha and Shaver (2011) were also applied (for further information on micrometeorological data processing see Euskirchen et al. (2012)). Once the data were processed, they were filtered using quality flag values from the instrumentation to select the best data available. In addition, soil heat flux plate measurements were corrected to account for soil heat storage above the plate according to the methodology of Domingo et al. (2000) and Lund et al. (2014) using existing field measurements of soil bulk density for each site (758 kg·m^{-3}, 989 kg·m^{-3} and 1038 kg·m^{-3} for Fen, Tussock and Heath flux stations, respectively). The final subset for evaluating the TSEB model was selected by imposing three criteria, identifying periods where: a) energy closure at the half-hourly timescale exceeded 70%, b) R_N was higher than 100 W·m^{-2} in order to ensure daylight conditions, and c) no precipitation present.

5 Accuracy and error estimation

The performance of the TSEB model and possible refinements for Arctic tundra was evaluated using the coefficient of determination (R^2); the root mean square error (RMSE), the mean bias error (MBE), the mean absolute difference (MAD) and the mean absolute percent difference (MAPD), from Eq. (19) to Eq. (23), respectively.

$$R^2 = \left(\frac{\sum_{i=1}^{n}(o_i-\bar{X})(e_i-\bar{Y})}{\sqrt{\sum_{i=1}^{n}(o_i-\bar{X})^2}\sqrt{\sum_{i=1}^{n}(e_i-\bar{Y})^2}} \right), \tag{19}$$

$$RMSE = \sqrt{\frac{\sum_{i=1}^{n}(e_i-o_i)^2}{n}}, \tag{20}$$

$$MBE = \frac{\sum_{i=1}^{n}(e_i-o_i)}{n}, \tag{21}$$

$$MAD = \frac{\sum_{i=1}^{n}|e_i-o_i|}{n}, \tag{22}$$

$$MAPD = \frac{100}{\bar{X}}\left(\frac{\sum_{i=1}^{n}|e_i-o_i|}{n}\right), \tag{23}$$

where e_i refers to the estimated value of the variable in question (R_N, H, LE or G), o_i is the observed value (*in situ* measurement provided by the flux station), n is the number of data points, and $\bar{X}$ and $\bar{Y}$ are the average of the o_i and e_i values, respectively.

6 Results and discussion

6.1 Soil heat flux estimation

Both the Kustas et al., (1998), K98, and the Santanello and Friedl (2003), SF03, soil heat flux models used to estimate G at the study sites yielded high errors when a value of $c_G = 0.3$ was used, with MAPD ranging from 90% to 159%, with the SF03 approach providing better results (Table 3). It is important to note that G is a relatively small term with a maximum value on the order of 50 W·m⁻². Both models generally overestimated G with a MBE from 3 W·m⁻² to 40 W·m⁻², with the SF03 model generating lower biases. Results improved when a c_G value of 0.14 was used with MAPD ranging from 48% to 76% and with lower RMSE values from 15 W·m⁻² to 21 W·m⁻² and MBE from -4 W·m⁻² to -14 W·m⁻². With the lower value of c_G, the K98 approach provided better results (Table 3).

Similar to the original c_G, c_{TG} can be also estimated using the Santanello and Friedl (2003) method in Eq. (17). Mean diurnal profiles in T_{RAD} and G, averaged over all tundra study sites, are shown in Fig. 2 demonstrating the observed relationships between these variables. The mean G value for the summer period peaked around 15:00 local solar time, with a phase shift around 4 hours after the maximum T_{RAD} at noon. Coefficients A, B and S were fitted using 60% of all available data, from 4 to 21 hours local solar time, with no restriction of balance closure, and the remaining 40% of the data were reserved for model testing. Using T_{RAD} and G observations at half-hourly timesteps from the fitting subset, diurnal c_{TG} curves were derived for the growing season for each of the tower sites, showing reasonable agreement (Fig. 3). A fit to the mean curve yielded parameter values of S = -14 400 seconds, A = 1.55 and B = 160 000 s. As in the case of Santanello and Friedl (2003), a B variation of ± 15 000 s had no significant influence on the results. Statistical comparisons between observed fluxes from the test subset and simulations using the fitted parameters show good agreement and negligible bias (Table 4), with R^2, MAPD, RMSE and MBE values of 0.68, 37%, 6 W·m⁻² and 0 W·m⁻², respectively. In addition, the new model was also evaluated using the same flux subset used in Table 3 to assess the K98 and SF03 configurations, demonstrating improved performance with roughly half the MAPD than K98 and SF03 configurations (Table 4).

To assess typical performance in a remote sensing application this new parameterization should be tested with satellite retrievals of T_{RAD}; the performance of the G parameterization for Arctic tundra reported here is comparable or superior to previous studies reported in the literature using the Santanello and Friedl (2003) or Kustas et al. (1998) appoaches for other ecosystems. In shrub-grass dominated areas and boreal forest several studies (Anderson et al., 2008;Kustas et al., 1998;Li et al., 2008;Sánchez et al., 2009;Timmermans et al., 2007) reported MAPD and RMSE values ranging from 19% to 59% and from 15 W·m⁻² to 35 W·m⁻², respectively. Studies in corn and soybean crops (Anderson et al., 2005;Choi et al., 2009;Li et al., 2005;Santanello and Friedl, 2003) reported MAPD and RMSE values ranging from 19% to 34% and from 10 W·m⁻² to 41 W·m⁻², respectively.

6.2 Net radiation estimation

Effective atmospheric emissivity estimated using the Brutsaert (1975) and Jin et al. (2006) methodologies yielded similar errors in simulated downwelling longwave radiation results, with a R^2 of 0.58 and a RMSE around 27 W·m^{-2}. The C coefficient computed through Jin et al. (2006) yielded a value of 1.25 ±0.009, very close to Brutsaert (1975) C value of 1.24. This suggests that the simpler Brutsaert (1975) C coefficient can be used efficiently to model effective atmospheric emissivity in all sky conditions when combined with Crawford and Duchon (1999) and Pons and Ninyerola (2008) methods for summer Arctic tundra.

Estimated R_N for all sky condition yielded strong agreement with observed values for all flux towers (see Fig. 4 and Table 5) with a mean R^2, MAPD, MAD, RMSE of 0.99, 7%, 18 W·m^{-2}, 23 W·m^{-2}, with a tendency to overestimate R_N with a MBE of 7 W·m^{-2}. In terms of RMSE and MAPD, all study sites behaved similarly (see Fig. 4). These results are in line with previous TSEB model applications for other cover types and clear sky conditions where a MAPD of around 5% was reported (Anderson et al., 2008;Li et al., 2005;Anderson et al., 2005;Kustas and Norman, 1999;Guzinski et al., 2013;Li et al., 2008;Anderson et al., 2000). This suggest that R_N estimation using this methodology scheme can be used to obtain reliable estimates of R_N under summer all sky conditions in Arctic tundra and can be applied regionally when a source of solar radiation (METEOSAT or GOES, Cristóbal and Anderson (2013), air temperature (Cristóbal et al., 2008) and T_{RAD} (MODIS Land Surface Temperature and emissivity product) are available.

6.3 Latent and sensible heat fluxes estimation

The average energy balance closure using half-hour periods for the evaluation subset was 88% which is in agreement with the average closure of 90% for these flux stations, (Euskirchen et al., 2012). Lack of closure may be explained by instrument and methodological uncertainties, insufficient estimation of storage terms, unmeasured advective fluxes, landscape scale heterogeneity or instrument spatial representativeness, among others (Lund et al., 2014;Stoy et al., 2013;Foken et al., 2011;Foken, 2008;Wilson et al., 2002). While, currently, there is no uniform answer how to deal with non-closure of the energy balance in eddy covariance datasets, and methods for analysing the reasons for the lack of closure are still under discussion (Foken et al., 2011). More recently there is evidence that non-orthogonal sonics underestimate vertical velocity causing under-measurement of H and LE on the order of 10%., (Kochendorfer et al., 2012; Frank et al., 2013) although this is still being debated (Kochendorfer et al., 2013). In the current study, a distribution of residual according to the Bowen ratio method was applied as suggested by Twine et al. (2000) and Foken (2008). In addition, LE was recalculated as the residual of the surface energy budget used in previous TSEB evaluations (Li et al., 2008); and both closure methods were then used to evaluate TSEB output.

Latent (LE) and sensible (H) heat estimated through both the new proposed soil heat flux methodology and the all sky R_N methodology scheme, yielded reasonable agreement with observed data using both closure methods (Bowen ratio (BR) and residual (RES)) at half-hourly timesteps for both α_{PTC} parameterizations of 0.92 and 1.26 (see Table 5 and 6 and Fig. 4 and

5),.; although α_{PTC} = 0.92 yielded marginally lower errors for the turbulent fluxes of H and LE. Relative errors (MAPD) were 34 and 27% for LE_{RES} and H, respectively, for all combined sites using α_{PTC} = 0.92, and 40 and 33% using the standard value of α_{PTC} = 1.26. Results with LE_{BR} and H_{BR} using α_{PTC} = 0.92 yielded MAPD of 42 and 36%, respectively, while using α_{PTC} = 1.26 yielded and 45 and 42%, respectively.

5 A slight improvement in H and LE estimates using α_{PTC} ~ 0.9 also agrees with Agam et al. (2010) who also found better results with lower α_{PTC} for natural vegetation in water limited environments. Nevertheless, since the mean RMSE for all fluxes and for all parameterizations and sites was around 50 W·m^{-2} (Table 5 and 6), which is commensurate with errors typically reported in other surface energy balance studies (Kalma et al., 2008), these results suggest that a generalized α_{PTC} value of 1.26 in global TSEB applications may adequately reproduce energy fluxes in Arctic tundra during the growing

10 season, from leaf-out until senescence, while also capturing inter- and intra-annual dynamics. However, biases in regional applications may be reduced by using a landcover class-dependent value of α_{PTC}.

Currently, there is limited research published on application of energy balance models to estimate energy fluxes for Arctic tundra. Mu et al. (2009) reported year-round errors from 20% to 40% in two Arctic tundra sites in Barrow (Alaska, USA) at daily periods based on a modified aerodynamic resistance–surface energy balance model where the required surface

15 conductance is estimated from remotely-sensed LAI based on Cleugh et al. (2007) formulation. TSEB results, however, were evaluated with half-hourly data in summer conditions and, although they cannot be directly compared with results in this previous study, they show similar errors. As in the case of R_N, LE and H results are also in line with previous works for other cover types using *in situ* data as input to TSEB (Anderson et al., 2000;Anderson et al., 2008;Li et al., 2005).

6.4 Seasonal dynamics of surface energy fluxes and energy partitioning

20 In general, monthly estimation of surface energy fluxes showed a good agreement with observations during the growing season. Because the model yielded similar results with both α_{PTC} parameterizations of 0.92 and 1.26, this section only shows the seasonal dynamics with α_{PTC} of 0.92. Estimated R_N yielded a low MAPD around 6%, increasing up to 12% at the end of the growing season (Table 7 and Fig. 6). The proposed new method to estimate G yielded better MAPD results from June to August which coincides with the peak of the growing season in July. A similar pattern was found for LE and H, where the

25 best MAPD results occurred also in the middle of the growing season (June and July). MAPD for LE, H and G tended to be higher in May and September; thus coinciding with earlier plant growth or the senesce periods, respectively. MODIS LAI product, used to estimate the fractional vegetation cover to partition soil and canopy temperatures, performed as a good proxy to capture inter- and intra-annual vegetation dynamics, performing well for the Arctic tundra and suggesting utility for regional applications (Fig. 7). However, f_G computed using PAR data did not show the same behaviour. While LAI captured

30 seasonal vegetation dynamics, with mean values ranging from 0.7 to 1.7 m^2·m^{-2}, f_G remained almost constant around 0.9, even at the early plant growth or the senesce periods. The presence of a variable organic layer, mainly composed of mosses

and lichens that remain green through all the season, might have masked the actual vegetation dynamics (Fig. 7). In addition, mosses may exert strong controls on understory water and heat fluxes in Arctic tundra ecosystems (Blok et al., 2011). The main effect over the model was to overestimate LE and underestimate H, yielding lower agreement with observed data in May and September. Guzinski et al. (2013) suggested a methodology based on EVI and NDVI indices successfully applied

5   to adjust f_G in crops, grasslands and forests; however, further research is needed to apply such methods for the Arctic tundra.

The pattern of daily estimated surface energy fluxes also compared well to observed fluxes for all sky conditions. As an example, time series of modelled and measured surface energy fluxes are segmented in Fig. 8 for the Heath flux station, with each diurnal segment representing flux data averaged by hour over 5-day intervals from 2008 to 2012. Observed and estimated R_N exhibited an excellent agreement showing almost the same daily temporal pattern for the full growing season

10   while LE, H and G yielded a good daily agreement being underestimated in May and September, especially in the case of LE.

In terms of observed ($_o$) and estimated ($_e$) mean season energy flux partitioning, LE_o/R_{No}, H_o/R_{No} and G_o/R_{No} yielded mean values of 0.55, 0.37 and 0.08, respectively; and LE_e/RN_e, H_e/R_{Ne} and G_e/R_{Ne} yielded mean values of 0.58, 0.34 and 0.08, respectively (Fig. 9). Observed and estimated Bowen ratio (β) yielded mean values of 0.50 and 0.67, respectively. In all

15   cases, observed and estimated results are in line with previous studies in the Arctic tundra (Lynch et al., 1999;Eugster et al., 2000). It is worth noting that the difference between observed and estimated values of LE/R_N, H/R_N partitions was only around 3% and for G/R_N was almost negligible. From June to August, mean absolute difference values between observed and estimated values for LE/R_N, H/R_N were around 4%, increasing up to 20% in September due to model over and underestimation, while G/R_N difference was only less than 1%.

20   These results suggest that the model is able to reproduce accurately temporal trends of energy partition in concert with tundra vegetation dynamics in the growing vegetation peak from June to August and could be used to monitor changes in surface energy fluxes concurrently with vegetation change.

7 Conclusions and future work

An extensive evaluation and refinements in R_N, G and α_{PTC} parameterizations of a two-source energy balance model (TSEB)

25   to estimate surface energy fluxes in different tundra types in Alaska for the full Arctic tundra growing season and its interannual dynamics from 2008 to 2012 in all-sky conditions was successfully performed. Although there are limited studies that model Arctic tundra surface energy fluxes, our results compared favourably to these studies conducted at similar sites. A mean RMSE value on the order of 50 W·m^{-2} in the turbulent heat fluxes is similar in magnitude to errors typically reported in other surface energy balance modelling studies and within the uncertainty in measured fluxes having 80-90%

30   closure. R_N estimation scheme applied in this work for all sky conditions yielded similar results as other studies for only clear sky conditions, showing its potential for regional scale applications when sources of solar radiation, air temperature and

T_{RAD} are available. The new model, developed to estimate soil heat flux (G) based on the T_S-G relationship was validated from the early growth to senescence using data for multiple years (hardly found in the literature); results displayed superior performance yielding half of the error of other models. Comparable error differences with both α_{PTC} parameterizations of 0.92 and 1.26 were found, suggesting that the original TSEB α_{PTC} of 1.26 for large area modelling is acceptable and valid for

5   the Arctic tundra. However, more research is needed to assess the influence of the organic layer on modelled results. The MODIS LAI product proved to be a reliable input for modelling energy fluxes in Arctic tundra in the absence of field data. Results also suggest that the model is able to reproduce accurately temporal trends of energy partitioning in concert with tundra vegetation dynamics in the peak growing season. Moreover, it also has potential to monitor changes in surface energy fluxes in Arctic tundra due to changes in vegetation composition (e.g., shrub encroachment) at regional scales using satellite

10   remote sensing data. This is particularly crucial in the Arctic where there is a sparse network of meteorological and flux observations Finally, further efforts will be focused on the daily energy flux integration by means of the implementation of the ALEXI/DisALEXI modelling system (Anderson et al., 2007; 2011), the dual-temperature-difference scheme (Norman et al., 2000; Guzinski et al., 2013), along with data fusion techniques (Cammalleri et al., 2013; 2014) schemes using additional satellite data such as Landsat, Terra/Aqua MODIS or NOAA AVHRR.

Acknowledgements

This research was supported by the Alaska NASA EPSCoR program awards NNX10NO2A and NNX13AB28A. Authors would also like to thank Colin Edgar from the Institute of Arctic Biology, UAF, for his help in data processing of the eddy covariance and meteorological data. Datasets from the Imnavait sites were provided by the Institute of Arctic Biology, UAF,

20   based upon work supported by the National Science Foundation under grant #1107892. USDA is an equal opportunity employer and provider.

References

ACIA: Impacts of a Warming Arctic, Cambridge University Press, Cambridge, 140 pp., 2004.

Agam, N., Kustas, W. P., Anderson, M. C., Norman, J. M., Colaizzi, P. D., Howell, T. A., Prueger, J. H., Meyers, T. P., and

25   Wilson, T. B.: Application of the Priestley–Taylor Approach in a Two-Source Surface Energy Balance Model, J Hydrometeorol, 11, 185-198, doi:10.1175/2009jhm1124.1, 2010.

AMAP: Arctic Climate Issues 2011: Changes in Arctic Snow, Water, Ice and Permafrost. SWIPA 2011. Overview Report, Oslo, Norway, 96 pp., 2012.

Anderson, M. C., Norman, J. M., Meyers, T. P., and Diak, G. R.: An analytical model for estimating canopy transpiration

30   and carbon assimilation fluxes based on canopy light-use efficiency, Agr Forest Meteorol, 101, 265-289, doi:10.1016/S0168-1923(99)00170-7, 2000.

Anderson, M. C., Norman, J. M., Mecikalski, J. R., Torn, R. D., Kustas, W. P., and Basara, J. B.: A multiscale remote sensing model for disaggregating regional fluxes to micrometeorological scales, J Hydrometeorol, 5, 343-363, 2004.

Anderson, M. C., Norman, J. M., Kustas, W. P., Li, F. Q., Prueger, J. H., and Mecikalski, J. R.: Effects of vegetation clumping on two-source model estimates of surface energy fluxes from an agricultural landscape during SMACEX, J Hydrometeorol, 6, 892-909, doi:10.1175/Jhm465.1, 2005.

Anderson, M. C., Kustas, W. P., and Norman, J. M.: Upscaling Flux Observations from Local to Continental Scales Using Thermal Remote Sensing, Agron J, 99, 240, doi:10.2134/agronj2005.0096S, 2007.

Anderson, M. C., Norman, J., Kustas, W., Houborg, R., Starks, P., and Agam, N.: A thermal-based remote sensing technique for routine mapping of land-surface carbon, water and energy fluxes from field to regional scales, Remote Sens Environ, 112, 4227-4241, doi:10.1016/j.rse.2008.07.009, 2008.

Anderson, M. C., Kustas, W. P., Norman, J. M., Hain, C. R., Mecikalski, J. R., Schultz, L., Gonzalez-Dugo, M. P., Cammalleri, C., d'Urso, G., Pimstein, A., and Gao, F.: Mapping daily evapotranspiration at field to continental scales using geostationary and polar orbiting satellite imagery, Hydrol Earth Syst Sc, 15, 223-239, doi:10.5194/hess-15-223-2011, 2011.

Anderson, M. C., Kustas, W. P., Alfieri, J. G., Gao, F., Hain, C., Prueger, J. H., Evett, S., Colaizzi, P., Howell, T., and Chávez, J. L.: Mapping daily evapotranspiration at Landsat spatial scales during the BEAREX'08 field campaign, Advances in Water Resources, 50, 162-177, doi:10.1016/j.advwatres.2012.06.005, 2012.

Arendt, A. A., Echelmeyer, K. A., Harrison, W. D., Lingle, C. S., and Valentine, V. B.: Rapid wastage of Alaska glaciers and their contribution to rising sea level, Science, 297, 382-386, doi:10.1126/science.1072497, 2002.

Bates, B. C., Kundzewicz, Z. W., S., W., and Palutikof, J. P.: Climate Change and Water, Technical Paper of the Intergovernmental Panel on Climate Change, Secretariat, Geneva., 2008.

Beringer, J., Chapin, F. S., Thompson, C. C., and McGuire, A. D.: Surface energy exchanges along a tundra-forest transition and feedbacks to climate, Agr Forest Meteorol, 131, 143-161, doi:10.1016/j.agrformet.2005.05.006, 2005.

Bhatt, U. S., Walker, D. A., Raynolds, M. K., Comiso, J. C., Epstein, H. E., Jia, G. S., Gens, R., Pinzon, J. E., Tucker, C. J., Tweedie, C. E., and Webber, P. J.: Circumpolar Arctic Tundra Vegetation Change Is Linked to Sea Ice Decline, Earth Interact, 14, 1-20, Artn 8. doi:10.1175/2010ei315.1, 2010.

Blok, D., Heijmans, M. M. P. D., Schaepman-Strub, G., van Ruijven, J., Parmentier, F. J. W., Maximov, T. C., and Berendse, F.: The Cooling Capacity of Mosses: Controls on Water and Energy Fluxes in a Siberian Tundra Site, Ecosystems, 14, 1055-1065, doi:10.1007/s10021-011-9463-5, 2011.

Boike, J., Hagedorn, B., and Roth, K.: Heat and Water Transfer Processes in Permafrost Affected Soils: A Review of Field and Modeling Based Studies for the Arctic and Antarctic, Plenary Paper, Proceedings of the 9th International Conference on Permafrost, June 29-July 3, 2008, University of Alaska, Fairbanks, USA, 2008a.

Boike, J., Wille, C., and Abnizova, A.: Climatology and summer energy and water balance of polygonal tundra in the Lena River Delta, Siberia, J Geophys Res-Biogeo, 113, Artn G03025, doi:10.1029/2007jg000540, 2008b.

Brutsaert, W.: On a derivable formula for long-wave radiation from clear skies, Water Resour Res, 11, 742-744, doi:10.1029/WR011i005p00742, 1975.

Cammalleri, C., Anderson, M. C., Ciraolo, G., D'Urso, G., Kustas, W. P., La Loggia, G., and Minacapilli, M.: The impact of in-canopy wind profile formulations on heat flux estimation in an open orchard using the remote sensing-based two-source model, Hydrol Earth Syst Sc, 14, 2643-2659, doi:10.5194/hess-14-2643-2010, 2010.

Cammalleri, C., Anderson, M. C., Ciraolo, G., D'Urso, G., Kustas, W. P., La Loggia, G., and Minacapilli, M.: Applications of a remote sensing-based two-source energy balance algorithm for mapping surface fluxes without in situ air temperature observations, Remote Sens Environ, 124, 502-515, doi:10.1016/j.rse.2012.06.009, 2012.

Cammalleri, C., Anderson, M. C., Gao, F., Hain, C. R., and Kustas, W. P.: A data fusion approach for mapping daily evapotranspiration at field scale, Water Resour Res, 49, 4672-4686, doi:10.1002/wrcr.20349, 2013.

Cammalleri, C., Anderson, M. C., Gao, F., Hain, C. R., and Kustas, W. P.: Mapping daily evapotranspiration at field scales over rainfed and irrigated agricultural areas using remote sensing data fusion, Agr Forest Meteorol, 186, 1-11, doi:10.1016/j.agrformet.2013.11.001, 2014.

Choi, M., Kustas, W. P., Anderson, M. C., Allen, R. G., Li, F., and Kjaersgaard, J. H.: An intercomparison of three remote sensing-based surface energy balance algorithms over a corn and soybean production region (Iowa, U.S.) during SMACEX, Agr Forest Meteorol, 149, 2082-2097, doi:10.1016/j.agrformet.2009.07.002, 2009.

Cleugh, H. A., Leuning, R., Mu, Q. Z., and Running, S. W.: Regional evaporation estimates from flux tower and MODIS satellite data, Remote Sens Environ, 106, 285-304, doi:10.1016/j.rse.2006.07.007, 2007.

Crawford, T. M., and Duchon, C. E.: An improved parameterization for estimating effective atmospheric emissivity for use in calculating daytime downwelling longwave radiation, J Appl Meteorol, 38, 474-480, doi:10.1175/1520-0450;2, 1999.

Cristóbal, J., Ninyerola, M., and Pons, X.: Modeling air temperature through a combination of remote sensing and GIS data, Journal of Geophysical Research, 113, 1-13, doi:10.1029/2007jd009318, 2008.

Cristóbal, J., and Anderson, M. C.: Validation of a Meteosat Second Generation solar radiation dataset over the northeastern Iberian Peninsula, Hydrol Earth Syst Sc, 17, 163-175, doi:10.5194/hess-17-163-2013, 2013.

Daughtry, C. S. T., Kustas, W. P., Moran, M. S., Pinter, P. J., Jackson, R. D., Brown, P. W., Nichols, W. D., and Gay, L. W.: Spectral Estimates of Net-Radiation and Soil Heat-Flux, Remote Sens Environ, 32, 111-124, doi:10.1016/0034-4257(90)90012-B, 1990.

Deardorff, J. W.: Efficient prediction of ground surface temperature and moisture, with inclusion of a layer of vegetation, Journal of Geophysical Research, 83, 1889, doi:10.1029/JC083iC04p01889, 1978.

Domingo, F., Villagarcia, L., Brenner, A. J., and Puigdefabregas, J.: Measuring and modelling the radiation balance of a heterogeneous shrubland, Plant Cell Environ, 23, 27-38, doi:10.1046/j.1365-3040.2000.00532.x, 2000.

Eaton, A. K., Rouse, W. R., Lafleur, P. M., Marsh, P., and Blanken, P. D.: Surface energy balance of the western and central Canadian subarctic: Variations in the energy balance among five major terrain types, J Climate, 14, 3692-3703, doi:10.1175/1520-0442, 2001.

Ekici, A., Chadburn, S., Chaudhary, N., Hajdu, L. H., Marmy, A., Peng, S., Boike, J., Burke, E., Friend, A. D., Hauck, C., Krinner, G., Langer, M., Miller, P. A., and Beer, C.: Site-level model intercomparison of high latitude and high altitude soil thermal dynamics in tundra and barren landscapes, Cryosphere, 9, 1343-1361, doi:10.5194/tc-9-1343-2015, 2015.

Elmendorf, S. C., Henry, G. H. R., Hollister, R. D., Bjork, R. G., Boulanger-Lapointe, N., Cooper, E. J., Cornelissen, J. H. C., Day, T. A., Dorrepaal, E., Elumeeva, T. G., Gill, M., Gould, W. A., Harte, J., Hik, D. S., Hofgaard, A., Johnson, D. R., Johnstone, J. F., Jonsdottir, I. S., Jorgenson, J. C., Klanderud, K., Klein, J. A., Koh, S., Kudo, G., Lara, M., Levesque, E., Magnusson, B., May, J. L., Mercado-Diaz, J. A., Michelsen, A., Molau, U., Myers-Smith, I. H., Oberbauer, S. F., Onipchenko, V. G., Rixen, C., Schmidt, N. M., Shaver, G. R., Spasojevic, M. J., Porhallsdottir, P. E., Tolvanen, A., Troxler, T., Tweedie, C. E., Villareal, S., Wahren, C. H., Walker, X., Webber, P. J., Welker, J. M., and Wipf, S.: Plot-scale evidence of tundra vegetation change and links to recent summer warming, Nat Clim Change, 2, 453-457, doi:10.1038/Nclimate1465, 2012.

Engstrom, R. N., Hope, A. S., Stow, D. A., Vourlitis, G. L., and Oechel, W. C.: Priestley-Taylor Alpha Coefficient: Variability and Relationship to Ndvi in Arctic Tundra Landscapes, J Am Water Resour As, 38, 1647-1659, doi:10.1111/j.1752-1688, 2002.

Eugster, W., Rouse, W. R., Pielke, R. A., McFadden, J. P., Baldocchi, D. D., Kittel, T. G. F., Chapin, F. S., Liston, G. E., Vidale, P. L., Vaganov, E., and Chambers, S.: Land-atmosphere energy exchange in Arctic tundra and boreal forest: available data and feedbacks to climate, Global Change Biol, 6, 84-115, doi:10.1046/j.1365-2486, 2000.

Eugster, W., McFadden, J. P., and Chapin, F. S.: Differences in Surface Roughness, Energy, and CO2 Fluxes in Two Moist Tundra Vegetation Types, Kuparuk Watershed, Alaska, U.S.A., 2005.

Euskirchen, E. S., Bret-Harte, M. S., Scott, G. J., Edgar, C., and Shaver, G. R.: Seasonal patterns of carbon dioxide and water fluxes in three representative tundra ecosystems in northern Alaska, Ecosphere, 3, art4, 10.1890/es11-00202.1, 2012.

Foken, T.: The energy balance closure problem: an overview, Ecol Appl, 18, 1351-1367, doi:10.1890/06-0922.1, 2008.

Foken, T., Aubinet, M., Finnigan, J. J., Leclerc, M. Y., Mauder, M., and U, K. T. P.: Results of a Panel Discussion About the Energy Balance Closure Correction for Trace Gases, B Am Meteorol Soc, 92, Es13-Es18, doi:10.1175/2011BAMS3130.1, 2011.

Frank, J. M., Massman, W. J., and Ewers, B. E.: Underestimates of sensible heat flux due to vertical velocity measurement errors in non-orthogonal sonic anemometers, Agr Forest Meteorol, 171, 72-81, doi:10.1016/j.agrformet.2012.11.005, 2013.

Guzinski, R., Anderson, M. C., Kustas, W. P., Nieto, H., and Sandholt, I.: Using a thermal-based two source energy balance model with time-differencing to estimate surface energy fluxes with day–night MODIS observations, Hydrol Earth Syst Sc, 17, 2809-2825, doi:10.5194/hess-17-2809-2013, 2013.

Hinzman, L. D., Goering, D. J., and Kane, D. L.: A distributed thermal model for calculating soil temperature profiles and depth of thaw in permafrost regions, J Geophys Res-Atmos, 103, 28975-28991, doi:10.1029/98jd01731, 1998.

Jacobsen, A., and Hansen, B. U.: Estimation of the soil heat flux net radiation ratio based on spectral vegetation indexes in high-latitude Arctic areas, Int J Remote Sens, 20, 445-461, doi:10.1080/014311699213532, 1999.

Jia, G. J., Epstein, H. E., and Walker, D. A.: Greening of arctic Alaska, 1981–2001, Geophys Res Lett, 30, 2067, doi:10.1029/2003gl018268, 2003.

Jiang, Y. Y., Rocha, A. V., O'Donnell, J. A., Drysdale, J. A., Rastetter, E. B., Shaver, G. R., and Zhuang, Q. L.: Contrasting soil thermal responses to fire in Alaskan tundra and boreal forest, J Geophys Res-Earth, 120, 363-378, doi:10.1002/2014JF003180, 2015.

Jin, X., Barber, D., and Papakyriakou, T.: A new clear-sky downward longwave radiative flux parameterization for Arctic areas based on rawinsonde data, J Geophys Res-Atmos, 111, Artn D24104. doi:10.1029/2005jd007039, 2006.

Jung, M., Reichstein, M., Ciais, P., Seneviratne, S. I., Sheffield, J., Goulden, M. L., Bonan, G., Cescatti, A., Chen, J., de Jeu, R., Dolman, A. J., Eugster, W., Gerten, D., Gianelle, D., Gobron, N., Heinke, J., Kimball, J., Law, B. E., Montagnani, L., Mu, Q., Mueller, B., Oleson, K., Papale, D., Richardson, A. D., Roupsard, O., Running, S., Tomelleri, E., Viovy, N., Weber, U., Williams, C., Wood, E., Zaehle, S., and Zhang, K.: Recent decline in the global land evapotranspiration trend due to limited moisture supply, Nature, 467, 951-954, doi:10.1038/nature09396, 2010.

Kade, A., Bret-Harte, M. S., Euskirchen, E. S., Edgar, C., and Fulweber, R. A.: Upscaling of CO_2fluxes from heterogeneous tundra plant communities in Arctic Alaska, Journal of Geophysical Research, 117, doi:10.1029/2012jg002065, 2012.

Kalma, J. D., McVicar, T. R., and McCabe, M. F.: Estimating Land Surface Evaporation: A Review of Methods Using Remotely Sensed Surface Temperature Data, Surv Geophys, 29, 421-469, doi:10.1007/s10712-008-9037-z, 2008.

Kane, D. L., Gieck, R. E., and Hinzman, L. D.: Evapotranspiration from a Small Alaskan Arctic Watershed, Nordic Hydrology, 21, 253-272, 1990.

Kane, D. L., Gieck, R. E., Kitover, D. C., Hinzman, L. D., Mcnamara, J. P., and Yang, D.: Hydrologic Cycle on the North Slope of Alaska, 2004.

Kane, D. L., and Yang, D.: Overview for Water Balance Determinations for High Latitude Watersheds, 2004.

Kodama, Y., Sato, N., Yabuki, H., Ishii, Y., Nomura, M., and Ohata, T.: Wind direction dependency of water and energy fluxes and synoptic conditions over a tundra near Tiksi, Siberia, Hydrol Process, 21, 2028-2037, doi:10.1002/hyp.6712, 2007.

Kongoli, C., Kustas, W. P., Anderson, M. C., Norman, J. M., Alfieri, J. G., Flerchinger, G. N., and Marks, D.: Evaluation of a Two-Source Snow–Vegetation Energy Balance Model for Estimating Surface Energy Fluxes in a Rangeland Ecosystem, J Hydrometeorol, 15, 143-158, doi:10.1175/jhm-d-12-0153.1, 2014.

Kustas, W. P., and Daughtry, C. S. T.: Estimation of the Soil Heat-Flux Net-Radiation Ratio from Spectral Data, Agr Forest Meteorol, 49, 205-223, doi:10.1016/0168-1923(90)90033-3, 1990.

Kustas, W. P., Zhan, X., and Schmugge, T. J.: Combining optical and microwave remote sensing for mapping energy fluxes in a semiarid watershed, Remote Sens Environ, 64, 116-131, doi:10.1016/S0034-4257(97)00176-4, 1998.

Kustas, W. P., and Norman, J. M.: Evaluation of soil and vegetation heat flux predictions using a simple two-source model with radiometric temperatures for partial canopy cover, Agr Forest Meteorol, 94, 13-29, doi:10.1016/S0168-1923(99)00005-2, 1999.

Kustas, W. P., and Norman, J. M.: A two-source energy balance approach using directional radiometric temperature observations for sparse canopy covered surfaces, Agron J, 92, 847-854, 2000.

Kochendorfer, J., Meyers, T. P., Frank, J., Massman, W. J., and Heuer, M. W.: How Well Can We Measure the Vertical Wind Speed? Implications for Fluxes of Energy and Mass, Bound-Lay Meteorol, 145, 383-398, doi:10.1007/s10546-012-9738-1, 2012.

Kochendorfer, J., Meyers, T. P., Frank, J. M., Massman, W. J., and Heuer, M. W.: Reply to the Comment by Mauder on "How Well Can We Measure the Vertical Wind Speed? Implications for Fluxes of Energy and Mass", Bound-Lay Meteorol, 147, 337-345, doi:10.1007/s10546-012-9792-8, 2012.

Lammers, R. B., Shiklomanov, A. I., Vorosmarty, C. J., Fekete, B. M., and Peterson, B. J.: Assessment of contemporary Arctic river runoff based on observational discharge records, J Geophys Res-Atmos, 106, 3321-3334, doi:10.1029/2000jd900444, 2001.

Langer, M., Westermann, S., Muster, S., Piel, K., and Boike, J.: The surface energy balance of a polygonal tundra site in northern Siberia - Part 1: Spring to fall, Cryosphere, 5, 151-171, doi:10.5194/tc-5-151-2011, 2011.

Li, F., Kustas, W. P., Anderson, M. C., Prueger, J. H., and Scott, R. L.: Effect of remote sensing spatial resolution on interpreting tower-based flux observations, Remote Sens Environ, 112, 337-349, doi:10.1016/j.rse.2006.11.032, 2008.

Li, F. Q., Kustas, W. P., Prueger, J. H., Neale, C. M. U., and Jackson, T. J.: Utility of remote sensing-based two-source energy balance model under low- and high-vegetation cover conditions, J Hydrometeorol, 6, 878-891, doi:10.1175/Jhm464.1, 2005.

Lund, M., Hansen, B. U., Pedersen, S. H., Stiegler, C., and Tamstorf, M. P.: Characteristics of summer-time energy exchange in a high Arctic tundra heath 2000-2010, Tellus B, 66, doi:10.3402/Tellusb.V66.21631, 2014.

Lynch, A. H., Chapin, F. S., Hinzman, L. D., Wu, W., Lilly, E., Vourlitis, G., and Kim, E.: Surface energy balance on the arctic tundra: Measurements and models, J Climate, 12, 2585-2606, doi:10.1175/1520-0442;2, 1999.

Massman, W. J.: A simple method for estimating frequency response corrections for eddy covariance systems, Agr Forest Meteorol, 104, 185-198, doi:10.1016/S0168-1923(00)00164-7, 2000.

Mendez, J., Hinzman, L. D., and Kane, D. L.: Evapotranspiration from a wetland complex on the Arctic coastal plain of Alaska, Nordic Hydrology, 29, 303-330, 1998.

Mu, Q. Z., Jones, L. A., Kimball, J. S., McDonald, K. C., and Running, S. W.: Satellite assessment of land surface evapotranspiration for the pan-Arctic domain, Water Resour Res, 45, Artn W09420 doi:10.1029/2008wr007189, 2009.

Myers-Smith, I. H., Forbes, B. C., Wilmking, M., Hallinger, M., Lantz, T., Blok, D., Tape, K. D., Macias-Fauria, M., Sass-Klaassen, U., Levesque, E., Boudreau, S., Ropars, P., Hermanutz, L., Trant, A., Collier, L. S., Weijers, S., Rozema, J., Rayback, S. A., Schmidt, N. M., Schaepman-Strub, G., Wipf, S., Rixen, C., Menard, C. B., Venn, S., Goetz, S., Andreu-Hayles, L., Elmendorf, S., Ravolainen, V., Welker, J., Grogan, P., Epstein, H. E., and Hik, D. S.: Shrub expansion in tundra ecosystems: dynamics, impacts and research priorities, Environmental Research Letters, 6, doi:10.1088/1748-9326/6/4/045509, 2011.

Norman, J. M., Kustas, W. P., and Humes, K. S.: Source Approach for Estimating Soil and Vegetation Energy Fluxes in Observations of Directional Radiometric Surface-Temperature, Agr Forest Meteorol, 77, 263-293, doi:10.1016/0168-1923(95)02265-Y, 1995.

Norman, J. M., Kustas, W. P., Prueger, J. H., and Diak, G. R.: Surface flux estimation using radiometric temperature: A dual-temperature-difference method to minimize measurement errors, Water Resour Res, 36, 2263, doi:10.1029/2000wr900033, 2000.

Overduin, P. P., and Kane, D. L.: Frost boils and soil ice content: Field observations, Permafrost Periglac, 17, 291-307, Doi 10.1002/Ppp.567, 2006.

Pons, X., and Ninyerola, M.: Mapping a topographic global solar radiation model implemented in a GIS and refined with ground data, Int J Climatol, 28, 1821-1834, doi:10.1002/Joc.1676, 2008.

Priestley, C. H. B., and Taylor, R. J.: On the assessment of surface heat flux and evaporation using large-scale parameters, Mon Weather Rev, 100, 81-92, 1972.

Rannik, Ü.: A comment on the paper by W.J. Massman 'A simple method for estimating frequency response corrections for eddy covariance systems', Agr Forest Meteorol, 107, 241-245, http://dx.doi.org/10.1016/S0168-1923(00)00236-7, 2001.

Rawlins, M. A., Steele, M., Holland, M. M., Adam, J. C., Cherry, J. E., Francis, J. A., Groisman, P. Y., Hinzman, L. D., Huntington, T. G., Kane, D. L., Kimball, J. S., Kwok, R., Lammers, R. B., Lee, C. M., Lettenmaier, D. P., McDonald, K. C., Podest, E., Pundsack, J. W., Rudels, B., Serreze, M. C., Shiklomanov, A., Skagseth, O., Troy, T. J., Vorosmarty, C. J., Wensnahan, M., Wood, E. F., Woodgate, R., Yang, D. Q., Zhang, K., and Zhang, T. J.: Analysis of the Arctic System for Freshwater Cycle Intensification: Observations and Expectations, J Climate, 23, 5715-5737, doi:10.1175/2010jcli3421.1, 2010.

Rocha, A. V., and Shaver, G. R.: Burn severity influences postfire CO2 exchange in arctic tundra, Ecol Appl, 21, 477-489, doi:10.1890/10-0255.1, 2011.

Romanovsky, V. E., Osterkamp, T. E., and Duxbury, N. S.: An evaluation of three numerical models used in simulations of the active layer and permafrost temperature regimes, Cold Reg Sci Technol, 26, 195-203, doi:10.1016/S0165-232x(97)00016-5, 1997.

Rouse, W. R.: Microclimate of Arctic Tree Line .2. Soil Microclimate of Tundra and Forest, Water Resour Res, 20, 67-73, doi:10.1029/Wr020i001p00067, 1984.

Sánchez, J. M., Caselles, V., Niclòs, R., Coll, C., and Kustas, W. P.: Estimating energy balance fluxes above a boreal forest from radiometric temperature observations, Agr Forest Meteorol, 149, 1037-1049, 10.1016/j.agrformet.2008.12.009, 2009.

Santanello, J. A., and Friedl, M. A.: Diurnal covariation in soil heat flux and net radiation, J Appl Meteorol, 42, 851-862, 2003.

Serreze, M. C., and Barry, R. G.: Processes and impacts of Arctic amplification: A research synthesis, Global Planet Change, 77, 85-96, doi:10.1016/j.gloplacha.2011.03.004, 2011.

Shutov, V., Gieck, R. E., Hinzman, L. D., and Kane, D. L.: Evaporation from land surface in high latitude areas: a review of methods and study results, Nordic Hydrology, 37, 393-411, doi:10.2166/Nh.2006.022, 2006.

Soegaard, H., Hasholt, B., Friborg, T., and Nordstroem, C.: Surface energy- and water balance in a high-arctic environment in NE Greenland, Theor Appl Climatol, 70, 35-51, doi:10.1007/s007040170004, 2001.

Stoy, P. C., Mauder, M., Foken, T., Marcolla, B., Boegh, E., Ibrom, A., Arain, M. A., Arneth, A., Aurela, M., Bernhofer, C., Cescatti, A., Dellwik, E., Duce, P., Gianelle, D., van Gorsel, E., Kiely, G., Knohl, A., Margolis, H., McCaughey, H., Merbold, L., Montagnani, L., Papale, D., Reichstein, M., Saunders, M., Serrano-Ortiz, P., Sottocornola, M., Spano, D., Vaccari, F., and Varlagin, A.: A data-driven analysis of energy balance closure across FLUXNET research sites: The role of landscape scale heterogeneity, Agr Forest Meteorol, 171, 137-152, doi:10.1016/j.agrformet.2012.11.004, 2013.

Sturm, M., Racine, C., and Tape, K.: Climate change. Increasing shrub abundance in the Arctic, Nature, 411, 546-547, doi:10.1038/35079180, 2001.

Tanner, C. B., and Jury, W. A.: Estimating evaporation and transpiration from a row crop during incomplete cover, Agron. J., 68, 239–242, 1976.

Timmermans, W. J., Kustas, W. P., Anderson, M. C., and French, A. N.: An intercomparison of the Surface Energy Balance Algorithm for Land (SEBAL) and the Two-Source Energy Balance (TSEB) modeling schemes, Remote Sens Environ, 108, 369-384, doi:10.1016/j.rse.2006.11.028, 2007.

Twine, T. E., Kustas, W. P., Norman, J. M., Cook, D. R., Houser, P. R., Meyers, T. P., Prueger, J. H., Starks, P. J., and Wesely, M. L.: Correcting eddy-covariance flux underestimates over a grassland, Agr Forest Meteorol, 103, 279-300, doi:10.1016/S0168-1923(00)00123-4, 2000.

Vörösmarty, C. J., Hinzman, L. D., Peterson, B. J., Bromwich, D. H., Hamilton, L. C., Morison, J., Romanovsky, V. E., Sturm, M., and Webb, R. S.: The Hydrologic Cycle and its Role in Arctic and Global Environmental Change: A Rationale and Strategy for Synthesis Study, Fairbanks, Alaska, 84 pp., 2001.

Webb, E. K., Pearman, G. I., and Leuning, R.: Correction of Flux Measurements for Density Effects Due to Heat and Water-Vapor Transfer, Q J Roy Meteor Soc, 106, 85-100, doi:10.1002/qj.49710644707, 1980.

Westermann, S., Luers, J., Langer, M., Piel, K., and Boike, J.: The annual surface energy budget of a high-arctic permafrost site on Svalbard, Norway, Cryosphere, 3, 245-263, 2009.

Wilson, K., Goldstein, A., Falge, E., Aubinet, M., Baldocchi, D., Berbigier, P., Bernhofer, C., Ceulemans, R., Dolman, H., Field, C., Grelle, A., Ibrom, A., Law, B. E., Kowalski, A., Meyers, T., Moncrieff, J., Monson, R., Oechel, W., Tenhunen, J., Valentini, R., and Verma, S.: Energy balance closure at FLUXNET sites, Agr Forest Meteorol, 113, 223-243, 2002.

Xu, L., Myneni, R. B., Chapin, F. S., Callaghan, T. V., Pinzon, J. E., Tucker, C. J., Zhu, Z., Bi, J., Ciais, P., Tommervik, H., Euskirchen, E. S., Forbes, B. C., Piao, S. L., Anderson, B. T., Ganguly, S., Nemani, R. R., Goetz, S. J., Beck, P. S. A., Bunn, A. G., Cao, C., and Stroeve, J. C.: Temperature and vegetation seasonality diminishment over northern lands, Nat Clim Change, 3, 581-586, doi:10.1038/Nclimate1836, 2013.

Yao, J. M., Zhao, L., Gu, L. L., Qiao, Y. P., and Jiao, K. Q.: The surface energy budget in the permafrost region of the Tibetan Plateau, Atmos Res, 102, 394-407, doi:10.1016/j.atmosres.2011.09.001, 2011.

Zhang, K., Kimball, J. S., Nemani, R. R., and Running, S. W.: A continuous satellite-derived global record of land surface evapotranspiration from 1983 to 2006, Water Resour Res, 46, Artn W09522, doi:10.1029/2009wr008800, 2010.

5 Zhang, Z., Kane, D. L., and Hinzman, L. D.: Development and application of a spatially-distributed Arctic hydrological and thermal process model (ARHYTHM), Hydrol Process, 14, 1017-1044, 2000.

Zhuang, Q., Romanovsky, V. E., and McGuire, A. D.: Incorporation of a permafrost model into a large-scale ecosystem model: Evaluation of temporal and spatial scaling issues in simulating soil thermal dynamics, J Geophys Res-Atmos, 106, 33649-33670, doi:10.1029/2001jd900151, 2001.
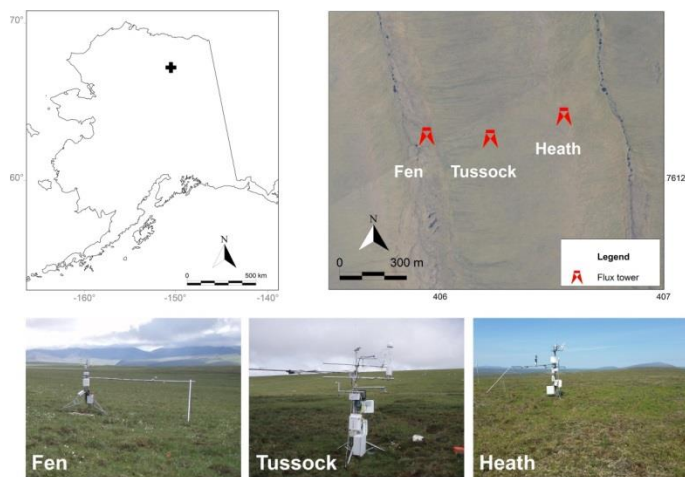
Figure 1: Location of the Fen, Tussock and Heath flux towers at Imnavait watershed. Right panel map is in UTM-6N NAD83 with coordinates in km.
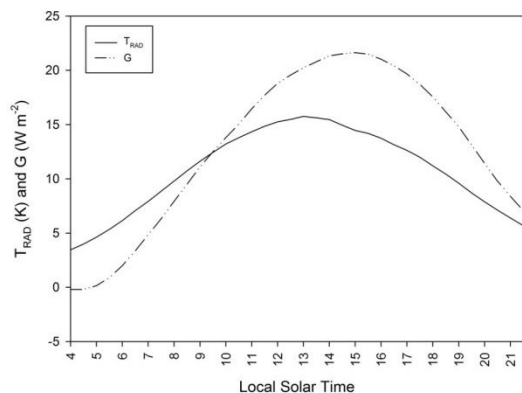
Figure 2. Mean daytime cycle for G and T$_{RAD}$ in the study area computed using all data available from the Fen, Tussock and Heath flux towers from 2008 to 2012.
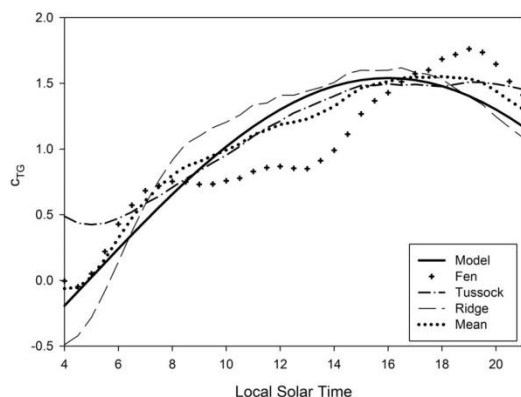
Figure 3. Time series of modeled c_{TG} and observed c_{TG} values from the Fen, Tussock and Heath flux stations as well as mean values for summer conditions.
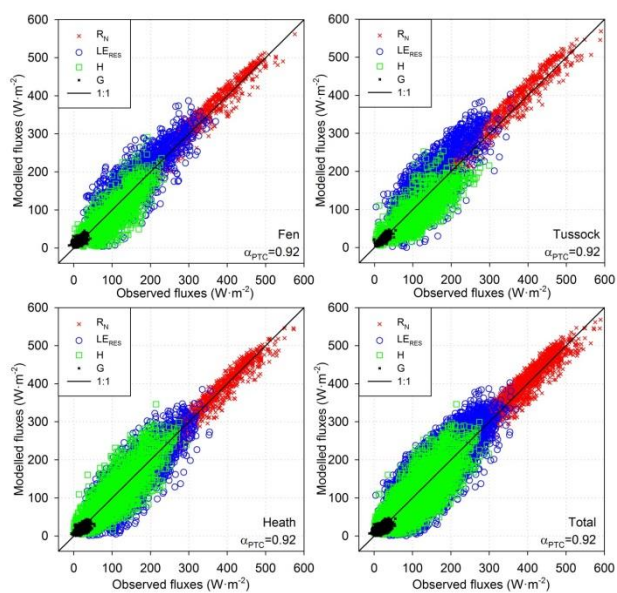
5   **Figure 4. Comparison of modeled vs. observed (using LE from residual closure) half-hourly surface fluxes using αPTC of 0.92. The 1:1 line represents perfect agreement with observations.**
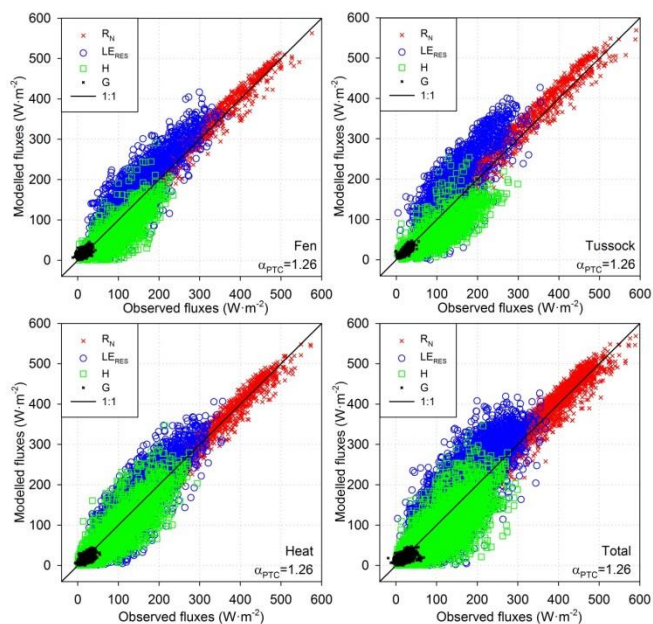
Figure 5. Comparison of modeled vs. observed (using LE from residual closure) half-hourly surface fluxes using αPTC of 1.26. The 1:1 line represents perfect agreement with observations.
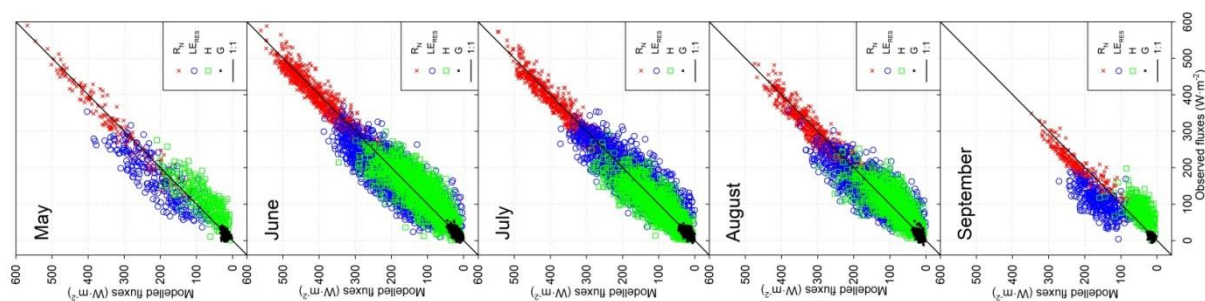
5 **Figure 6. Comparison of modeled vs. observed (using LE from residual closure) half-hourly surface fluxes by month using αPTC of 0.92 and G estimated by the new model. The 1:1 line represents perfect agreement with observations.**
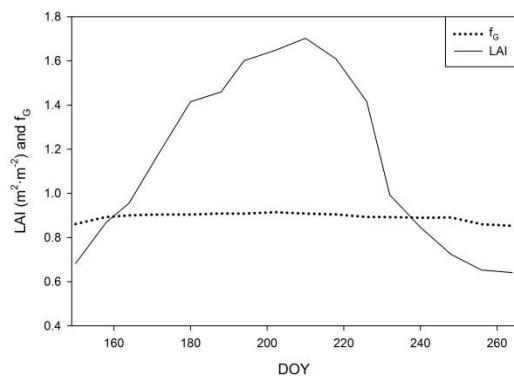
Figure 7. Mean MODIS LAI and f_G temporal dynamics for all flux stations from 2008 to 2012 averaged by 8-day intervals.
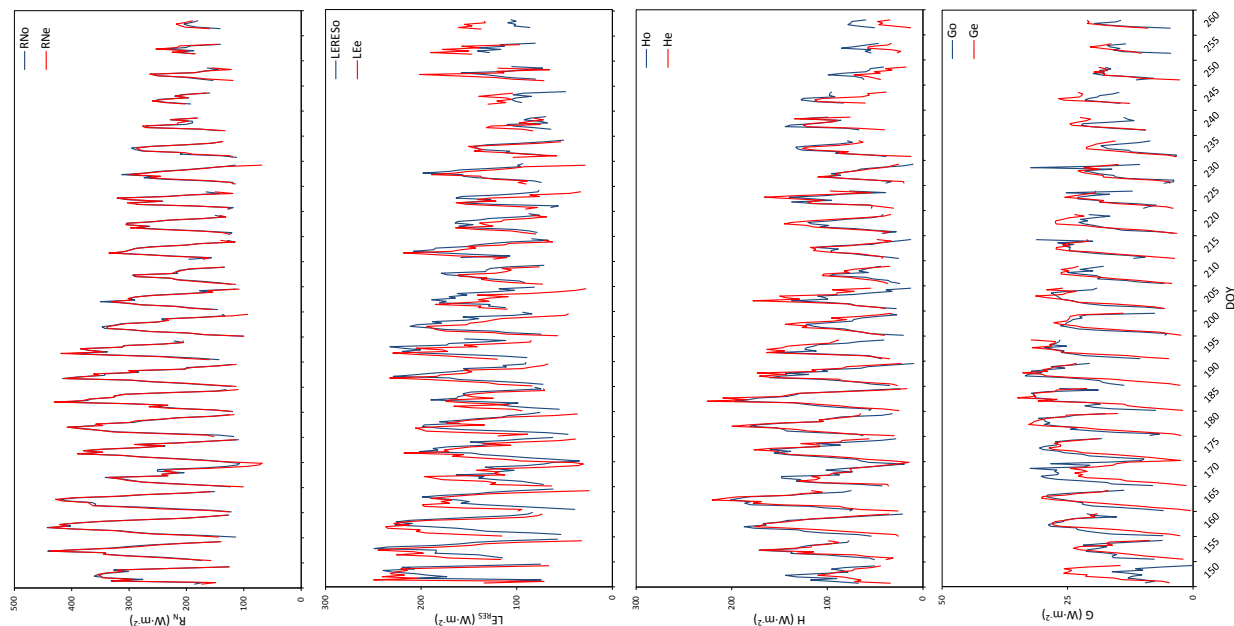
Figure 8. Comparison of hourly flux tower RN, LE, H and G observations (using LE from residual closure) (o) (from 6 to 21 hours local solar time) at the Heath flux tower with model estimates (e) using αPTC of 0.92. Each diurnal segment represents flux data averaged by hour over 5-day intervals from 2008 to 2012.
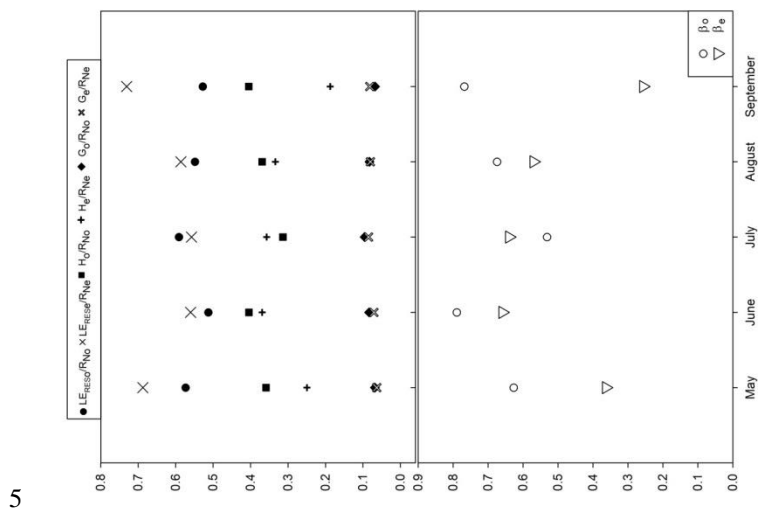
Figure 9. Monthly mean observed (o) and estimated (e) energy partitioning (LE/RN, H/RN and G/RN) and Bowen ratio (β) for all flux stations from 2008 to 2012 using αPTC of 0.92. LE observed values computed using the residual closure method.

Flux station name			Fen	Tussock	Heath
Coordinates (lat, long - WGS84)			68.606, -149.311	68.606, -149.304	68.607, -149.296
Period (Year|Day of Year)			2008|194-252	2009|194-253	2008|194-252
			2010|142-262	2010|142-262	2009|159-253
			2011|217-262	2012|156-226	2010|143-262
			2012|153-264		2011|147-262
					2012|156-226
TSEB inputs	**Symbol**	**Units**			
Wind speed	u	m s^{-1}	3.3 ± 1.7	3.4 ± 1.4	3.4 ± 1.4
Air temperature	T_a	°C	11.6 ± 3.5	12.8 ± 3.8	12.8 ± 3.8
Vapor pressure	e_a	kPa	0.9 ± 0.2	1 ± 0.3	1 ± 0.3
Atmospheric pressure	P	kPa	92 ± 0.2	90 ± 0.6	90 ± 0.6
Solar radiation	S_d	W·m^{-2}	432 ± 121	503 ± 149	503 ± 149
Longwaveincoming radiation	L_d	W·m^{-2}	261 ± 37	245 ± 34	245 ± 34
Surface temperature	T_s	K	288 ± 4	290 ± 5	290 ± 6
Leaf area index (MODIS)	LAI	m^2·m^{-2}	1.15 ± 0.32	1.28 ± 0.42	1.25 ± 0.4
Canopy height	h_c	m	0.4	0.4	0.4
Clumping factor	Ω_c		1	1	1
Fraction of green vegetation	f_g		0.92 ± 0.01	0.9 ± 0.03	0.9 ± 0.03

Table 1. Flux station name and location, period of model evaluation and list of inputs required by the TSEB. Average and standard deviation for the input values were computed for each period and for each site.

Instrument	Description	Height/*Depth*(m)
Campbell Sci. CSAT3	Three Dimensional Sonic Anemometer	2.18 - 3.18
Licor LI-7500	Open Path Infrared Gas Analyzer (CO2 and H2O)	2.18 - 3.18
Vaisalla HMP45C	Temperature and Relative Humidity Probe	1.93 - 2.82
Hukseflux HFP0SC	Soil Heat Flux Plate	*0.08*
Campbell Sci. TCAV	Type E Thermocouple Averaging Soil Temperature Probe	*0.02*
Campbell Sci. CS616	Water Content Reflectometer	*0.025*
Licor LI190SB	PAR Sensor (incoming)	2 - 3.6
Licor LI190SB	PAR Sensor (outgoing)	2
Met One Ins. 014A	Wind Speed Sensor	1.5 - 2.26
Kipp & Zonen CMA6	Pyranometer/Albedometer	2
*Kipp & Zonen CNR4	Four components net Radiometer	2
Kipp & Zonen NR-Lite	Net radiation	2
Apogee IRR-P	InfraRed Radiometer Sensor	1.5 - 3

Table 2. General overview of the Fen, Tussock and Heath flux sites instrumentation (more information available at: http://aon.iab.uaf.edu/imnavait). Apogee infrared radiometers were oriented 45º off-nadir at the three flux stations. Asterisk (*) means that this instrument is only available at the Tussock flux station.

			SF03					K98				
	c_G	n	R^2	RMSE	MBE	MAD	MADP	R^2	RMSE	MBE	MAD	MADP
Fen	0.30	1558	0.04	23	3	20	128	0.01	40	23	31	199
	0.14		0.04	15	-7	12	76	0.01	15	2	11	73
Tussock	0.30	1273	0.18	23	3	18	78	0.05	39	21	32	138
	0.14		0.23	17	-11	12	53	0.05	15	-4	11	46
Heath	0.30	2347	0.11	26	-5	20	96	0.10	34	14	26	125
	0.14		0.14	21	-14	15	72	0.06	16	-5	10	48
Total	0.30	5178	0.12	25	0	20	98	0.03	37	19	29	145
	0.14		0.10	18	-11	14	68	0.03	15	-3	11	53

Table 3. Performance statistics for the soil heat flux estimation using Santanello and Friedl (2003), SF03, and Kustas et al. (1998), K98, methodologies and two values for the maximum c_G value. RMSE, MBE and MAD are in W·m^{-2} and MADP in %.

	Fit subset (60%)				Test subset (40%)				Flux subset			
	Fen	Tussock	Heath	Total	Fen	Tussock	Heath	Total	Fen	Tussock	Heath	Total
R^2	0.89	0.99	0.99	0.99	0.55	0.77	0.69	0.68	0.27	0.56	0.49	0.44
RMSE	3.9	1	1	1	7	5	6	6	9	5	7	7
MBE	1.7	-0.2	-0.6	0.1	0.6	-0.3	-0.3	0	3.9	0.5	-0.3	1
MAD	2.8	1	1	1	5	4	5	4	7	4	5	6
MAPD	25	8	8	8	49	28	38	37	44	17	24	28
n	8283	10332	10748	29363	3310	4122	4273	11705	1558	1273	2347	5178

Table 4. Accuracy statistic for the new c_{TG} approach for the fit, the test and the flux subset used for Table 3. RMSE, MBE and MAD in W·m^{-2}, MADP in % and n is number of half-hour intervals.

			R_N			
	n	R^2	RMSE	MBE	MAD	MAPD
Fen	1558	0.99	23	8	18	7
Tussock	1273	0.99	25	12	19	7
Heath	2347	0.99	20	2	15	6
Total	5178	0.99	23	7	18	7

			LE_{BR}							LE_{RE}			
	n	R^2	RMSE	MBE	MAD	MAPD		n	R^2	RMSE	MBE	MAD	MAPD
Fen	1558	0.76	53	35	44	42	Fen	1558	0.75	41	15	33	31
Tussock	1273	0.67	59	43	50	45	Tussock	1273	0.69	54	32	45	40
Heath	2347	0.65	49	22	39	38	Heath	2347	0.67	41	0	32	31
Total	5178	0.70	53	31	43	42	Total	5178	0.68	44	12	35	34

			H							H_{BR}			
	n	R^2	RMSE	MBE	MAD	MAPD		n	R^2	RMSE	MBE	MAD	MAPD
Fen	1558	0.66	31	-12	24	25	Fen	1558	0.68	47	-32	37	39
Tussock	1273	0.65	39	-18	31	29	Tussock	1273	0.66	52	-35	40	37
Heath	2347	0.72	34	1	27	27	Heath	2347	0.72	45	-21	34	34
Total	5178	0.67	35	-7	27	27	Total	5178	0.68	46	-26	36	36

5 **Table 5.** Accuracy and error statistics from the comparison of modelled vs. observed surface fluxes using αPTC of 0.92. n is the number of half-hour periods analysed. RMSE, MAD and MBE are in W·m^{-2} and MADP in %. Subscripts BR and RES are Bowen ratio and residual closure methods, respectively.

			R_N			
	n	R^2	RMSE	MBE	MAD	MAPD
Fen	1558	0.99	23	8	18	7
Tussock	1273	0.99	25	12	19	7
Heath	2347	0.99	20	2	15	6
Total	5178	0.99	23	7	18	7

			LE_{BR}							LE_{RE}			
	n	R^2	RMSE	MBE	MAD	MAPD		n	R^2	RMSE	MBE	MAD	MAPD
Fen	1558	0.73	58	44	49	47	Fen	1558	0.77	49	30	41	39
Tussock	1273	0.65	63	48	55	47	Tussock	1273	0.71	61	40	47	42
Heath	2347	0.63	55	34	46	44	Heath	2347	0.70	45	16	36	35
Total	5178	0.66	58	38	48	45	Total	5178	0.71	53	28	43	40

			H							H_{BR}			
	n	R^2	RMSE	MBE	MAD	MAPD		n	R^2	RMSE	MBE	MAD	MAPD
Fen	1558	0.61	40	-26	32	33	Fen	1558	0.63	52	-40	44	45
Tussock	1273	0.59	46	-29	34	32	Tussock	1273	0.60	54	-36	43	39
Heath	2347	0.67	38	-13	30	30	Heath	2347	0.67	50	-31	40	40
Total	5178	0.62	42	-22	33	33	Total	5178	0.64	50	-34	40	42

Table 6. Accuracy and error statistics from the comparison of modelled vs. observed surface fluxes using αPTC of 1.26. n is the number of half-hour periods analysed. RMSE, MAD and MBE are in W·m^{-2} and MADP in %. Subscripts BR and RES are Bowen ratio and residual closure methods, respectively.

			R_N					LE			
	n	R^2	RMSE	MBE	MAD	MADP	R^2	RMSE	MBE	MAD	MADP
May	227	0.99	24	7	19	7	0.76	54	35	45	39
June	1727	0.99	22	6	17	6	0.73	46	19	37	33
July	1647	0.99	21	5	17	6	0.71	40	-3	31	27
August	1264	0.99	23	6	19	8	0.64	41	10	33	37
September	312	0.99	26	14	23	12	0.43	59	45	52	69

			H					G			
	n	R^2	RMSE	MBE	MAD	MADP	R^2	RMSE	MBE	MAD	MADP
May	227	0.68	42	-29	34	31	0.12	10	1	8	48
June	1727	0.70	37	-13	29	23	0.45	7	0	6	26
July	1647	0.72	31	7	24	28	0.49	6	1	5	23
August	1264	0.60	33	-8	25	28	0.40	7	3	6	34
September	312	0.30	43	-35	37	46	0.27	7	4	5	40

Table 7. Mean monthly accuracy and error statistics from the comparison of modelled vs. observed surface fluxes (using LE from residual closure) using αPTC of 0.92. n is the number of half-hour periods analysed. RMSE, MAD and MBE are in W·m^{-2} and MADP in %.